reduction or an increase in coherence of illumination of the collectors took place. Therefore, time spectra with counting rates outside these limits were discarded.

To prove antibunching, a total of four spectra were accumulated for about 30 h each. The first spectrum was for incoherent illumination of the detectors; the next three spectra were, respectively, for partially coherent, totally coherent and then again for partially coherent illumination. The evaluation procedure of the experimental time spectra consisted of smoothing and normalizing the spectra, followed by visually superimposing the incoherent with the coherent and partially coherent spectra, respectively. The results are summarized in Fig. 3 and Table 1. The antibunching signal S, that is, the missing coincidences ΔN in the coherent and partially coherent spectra versus the incoherent spectrum, becomes visible as a flattening of the peak in Fig. 3 within the time resolution window of ± 13 ps. The measured relative reduction in coincidences amounts to $S_{rel} = 1.26 \times 10^{-3}$ with a signal-to-noise ratio of 3. This agrees with the theoretically expected value calculated from the characteristic features of our cold tungsten field emitter. As expected, the reduction in coincidence rate and the signal-to-noise ratio are smaller for partially coherent illumination.

Antibunching—in general, interference between two particles (second order coherence)—has now been observed for massive free particles. This experimental technique opens a gateway to new fundamental tests of quantum mechanics and statistics: for example, observation of quantum statistics on interference phenomena, and experimental tests of interaction of fields and potentials with charged two-fermion systems[16–19]. □

Received 26 April; accepted 12 June 2002; doi:10.1038/nature00911.

1. Hanbury Brown, R. & Twiss, R. Q. A new type of interferometer for use in radio astronomy. *Phil. Mag.* **45,** 663–682 (1954).
2. Hanbury Brown, R. & Twiss, R. Q. Correlation between photons in two coherent beams of light. *Nature* **177,** 27–29 (1956).
3. Hanbury Brown, R. & Twiss, R. Q. The question of correlation between photons in coherent light rays. *Nature* **178,** 1447–1448 (1956).
4. Hanbury Brown, R. & Twiss, R. Q. Interferometry of the intensity fluctuation in light I. *Proc. R. Soc. Lond.* **242,** 300–324 (1957).
5. Hanbury Brown, R. & Twiss, R. Q. Interferometry of the intensity fluctuation in light II. An experimental test of the theory for partially coherent light. *Proc. R. Soc. Lond.* **243,** 291–319 (1958).
6. Purcell, E. M. The question of correlation between photons in coherent light rays. *Nature* **178,** 1449–1450 (1956).
7. Brannen, E. & Ferguson, H. I. S. The question of correlation between photons in coherent light beams. *Nature* **178,** 481–482 (1956).
8. Hanbury Brown, R. *The Intensity Interferometer* 7 (Taylor and Francis, New York, 1974).
9. Hanbury Brown, R. & Twiss, R. Q. A test of a new type of stellar interferometer on Sirius. *Nature* **178,** 1046–1448 (1956).
10. Silverman, M. P. On the feasibility of observing electron antibunching in a field-emission beam. *Phys. Lett. A* **120,** 442–446 (1987).
11. Kodama, T. *et al.* Feasibility of observing two-electron interference. *Phys. Rev. A* **57,** 2781–2785 (1998).
12. Henny, M. *et al.* The fermionic Hanbury Brown and Twiss experiment. *Science* **284,** 296–298 (1999).
13. Oliver, W. D., Kim, J., Liu, R. C. & Yamamoto, Y. Hanbury Brown and Twiss-type experiment with electrons. *Science* **284,** 299–301 (1999).
14. Twiss, R. Q. & Little, A. G. The detection of time-correlated photons by a coincidence counter. *Aust. J. Phys.* **12,** 77–93 (1959).
15. Hasselbach, F. A ruggedized miniature UHV electron biprism interferometer for new fundamental experiments and applications. *Z. Phys. B* **71,** 443–449 (1988).
16. Goldberger, M. L., Lewis, H. W. & Watson, K. M. Use of intensity correlations to determine the phase of a scattering amplitude. *Phys. Rev.* **132,** 2764–2787 (1963).
17. Silverman, M. P. New quantum effects of confined magnetic flux on electrons. *Phys. Lett. A* **118,** 155–158 (1986).
18. Silverman, M. P. in *OSA Proceedings on Photon Correlation Techniques and Applications* (eds Abbiss, J. B. & Smart, E. A.) Vol. 1 26–34 (OSA, Washington DC, 1988).
19. Silverman, M. P. Distinctive quantum features of electron intensity correlation interferometry. *Il Nuovo Cimento* **97,** 200–219 (1987).

Acknowledgements

We thank M. Silverman, M. Lenc, T. Tyc, A. Oed and P. Sonnentag for discussions, and the Deutsche Forschungsgemeinschaft for financial support.

Competing interests statement

The authors declare that they have no competing financial interests.

Correspondence and requests for materials should be addressed to F.H. (e-mail: franz.hasselbach@uni-tuebingen.de).

The energy efficiency of formation of photons, radicals and ions during single-bubble cavitation

Yuri T. Didenko & Kenneth S. Suslick

Department of Chemistry, University of Illinois at Urbana-Champaign, Urbana, Illinois 61801, USA

It is extremely difficult to perform a quantitative analysis of the chemistry[1,2] associated with multibubble cavitation: unknown parameters include the number of active bubbles, the acoustic pressure acting on each bubble and the bubble size distribution. Single-bubble sonoluminescence[3–7] (characterized by the emission of picosecond flashes of light) results from nonlinear pulsations of an isolated vapour-gas bubble in an acoustic field. Although the latter offers a much simpler environment in which to study the chemical activity of cavitation, quantitative measurements have been hindered by the tiny amount of reacting gas within a single bubble (typically $<10^{-13}$ mol). Here we demonstrate the existence of chemical reactions within a single cavitating bubble, and quantify the sources of energy dissipation during bubble collapse. We measure the yields of nitrite ions, hydroxyl radicals and photons. The energy efficiency of hydroxyl radical formation is comparable to that in multibubble cavitation, but the energy efficiency of light emission is much higher. The observed rate of nitrite formation is in good agreement with the calculated diffusion rate of nitrogen into the bubble. We note that the temperatures attained in single-bubble cavitation in liquids with significant vapour pressures will be substantially limited by the endothermic chemical reactions of the polyatomic species inside the collapsing bubble.

Single-bubble sonoluminescence (SBSL)[3,4] has attracted much attention owing to both the apparent simplicity of its creation and the complexity of processes occurring during bubble pulsation. A single bubble of gas can be trapped in partially degassed liquid by a standing acoustic wave and driven into highly nonlinear pulsations. At appropriate acoustic intensities, the bubble can emit short (~50–

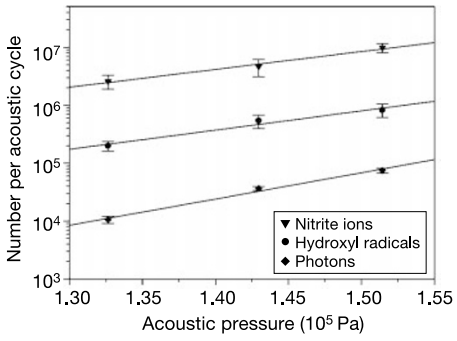

Figure 1 The yields of nitrite ions, hydroxyl radicals, and photons from a single cavitating bubble at 52 kHz in a 15-ml glass cell at 3 °C. The SBSL apparatus is described elsewhere[26]. Solutions of 10^{-3} M disodium terephthalate in high-purity water were used to measure the yields of hydroxyl radicals. Liquid was degassed and equilibrated with an air pressure of 150 torr. The fluorescence of the product, 2-hydroxyterephthalate, was measured at 425 nm (excitation: 315 nm)[27]. 2-hydroxyterephthalic acid was synthesized[28] and used as a standard after calibration for the $OH^{\bullet}$ trapping efficiency[29]. The yields of NO_2^- were measured from the fluorescence at 405 nm (excitation: 365 nm) of the product of reaction of NO_2^- with 2,3-diaminonaphthalene[30]. The acoustic pressure at the position of the bubble was measured with a needle hydrophone (DAPCO), which was calibrated against a Bruel and Kjaer 8103 hydrophone[31].

500 ps) flashes[6,7] of light with clock-like regularity[5]. The featureless spectra of SBSL from 200 to 800 nm with the increasing intensity toward the ultraviolet[6,8] suggested the existence of extraordinary temperatures inside the bubble, with black-body effective temperatures[8] as high as ~20,000 K. Ionization of the bubble contents would also occur at these temperatures, so SBSL is now generally believed to be due, at least in part, to black-body radiation, bremsstrahlung and ion–electron recombination processes[8–10].

Before the discovery of SBSL, research on sonoluminescence and sonochemistry was limited to studies of clouds of cavitating bubbles formed in high-intensity ultrasound field[1,2]. Using sensitive fluorescent analyses, we now report the yields of hydroxyl radicals ($OH^{\bullet}$) and nitrite ions (NO_2^-) from a single cavitation bubble. This allowed us to determine energetic characteristics of sonochemical activity of acoustic cavitation. We also present quantitative comparisons between single-bubble sonochemical rates and sonoluminescence intensity.

A bubble pulsating in water containing dissolved air is thought to contain primarily argon, because the N_2, O_2 and H_2O that diffuse into the bubble during expansion should burn off to form soluble products during bubble compression: the "dissociation hypothesis"[11]. The expected initial products of chemical reactions inside the bubble include $OH^{\bullet}$ and nitrogen oxides (NO_x). $OH^{\bullet}$ will react with organic compounds in the water or dimerize to H_2O_2, and NO_x will react with water giving nitrite and nitrate ions.

The formation of $OH^{\bullet}$ in multibubble sonochemistry of water was predicted more than 50 years ago and measured quantitatively using EPR spin-trap methods[12]. The formation of nitrite and nitrate ions in multibubble sonochemistry has also been measured, and the yield of NO_3^- is much lower than NO_2^- (ref. 13).

We have now measured the yields of $OH^{\bullet}$ and NO_2^- from a single cavitating bubble in water at 28 and 52 kHz, and at 3 °C and 22 °C. Most experiments were conducted at 52 kHz, as the smaller cell volume gives a higher concentration of products. Spectra of SBSL were collected under identical conditions, and a direct correlation between the yields of photons and chemical products was observed. In order to quantify gas diffusion processes, we also measured the size of the cavitating bubble throughout its cycle by a direct stroboscopic method[14]. The yields of photons, $OH^{\bullet}$, and NO_2^- increase with increasing acoustic intensity, and the yields of $OH^{\bullet}$ and NO_2^- are substantially higher than the number of photons emitted (Fig. 1).

Our data allow a meaningful estimate of the yield of radicals and ions per joule of absorbed energy (that is, a G value) for acoustic cavitation. From Table 1, the G value for $OH^{\bullet}$ formation during single bubble cavitation is 1×10^{-10} mol J^{-1} comparable to 3×10^{-10} mol J^{-1} for multibubble sonochemistry[15], but much less than typical radiolysis G values of 3×10^{-7} mol J^{-1}. Previous reports of G values for multibubble sonochemistry[15] are difficult to interpret because the absorbed acoustic energy is distributed among all bubbles in the cloud to varying degrees, and not exclusively to the few strongly cavitating bubbles that are chemically active at any one time.

The potential energy possessed by a single bubble[16] at its maximum size, R_{max}, is the upper limit of the energy available for the formation of radicals and ions. During bubble compression, the potential energy of the bubble is converted into mechanical energy (both bubble/liquid wall motion and shock waves into the liquid), heat, chemical reactions and light emission. The data in Table 1 on the yields of photons, radicals and ions can be used to calculate the energy balance of a collapsing bubble. From the endothermicity of the sonochemical reactions, we estimate that $\sim 1 \times 10^{-4}$ of potential energy of the bubble goes to the formation of radicals and ions that escape the collapsing bubble, and that the energy of the photons is another factor of 100 less.

This represents, however, only the lower limit of chemical reactions within the bubble. Substantial recombination of radicals or ions must occur inside the collapsing bubble and will be converted to heat[17]. For a 30-μm-radius bubble containing 0.01 bar of water vapour, there are $\sim 2.6 \times 10^{10}$ water molecules present; to dissociate all of these to hydrogen and oxygen atoms would require $\sim 2.5 \times 10^{11}$ eV, that is, several times the total potential energy of the bubble. It is likely, therefore, that sonochemical reactions within the bubble are the primary limiter of the efficiency of the bubble collapse.

Spectra of SBSL were collected under identical conditions to those used for the chemical analyses. As shown in Figs 2 and 3, the spectral distribution of SBSL does not change with an increase in acoustic intensity or of frequency. However, the spectra of sonoluminescence are dependent on the water temperature. This effect has been previously reported for different gases dissolved in water[4,18]. The ultraviolet component of SBSL is significantly less intense at 22 °C even though the overall SBSL intensity is the same or even higher at 22 °C compared to 3 °C (Figs 2 and 3). It is worth noting that our measured energy efficiency of photon production by SBSL is ~10^4 higher than that estimated grossly for multibubble sonoluminescence[19]. In SBSL, substantial emission of deep-ultraviolet photons that are absorbed by the liquid is likely to occur; this means that our estimate of the energy efficiency of photon production is only a lower limit.

Table 1 Quantitative sonochemistry in a single cavitation bubble at 52 kHz

Conditions	22 °C	3 °C
R_{max}, μm*	28.9	30.5
Number of $OH^{\bullet}$ radicals per cycle	6.6×10^5	8.2×10^5
Number of photons per cycle	8.1×10^3	7.5×10^4
Number of NO_2^- ions per cycle	3.7×10^6	9.9×10^6
Potential energy at R_{max} (eV)	6.4×10^{10}	7.5×10^{10}
Energy to form $OH^{\bullet}$ radicals (eV per cycle)†	3.4×10^6	4.3×10^6
Energy to form NO_2^- ions (eV per cycle)†	1.6×10^6	4.2×10^6
Energy of photons (200–750 nm) (eV per cycle)	2.7×10^4	2.6×10^5
Energy efficiency of sonoluminescence‡	4.3×10^{-7}	3.5×10^{-6}
Energy efficiency of sonochemistry§	7.8×10^{-5}	1.1×10^{-4}

*Experimentally observed (see text). Acoustic pressure: 1.5 atm.
†From the enthalpy of formation of $H_2O \rightarrow OH^{\bullet} + H^{\bullet}$ and of $2H_2O + 2N_2 + O_2 \rightarrow 4HNO_2$ in the gas phase at 273 K and 1 atm, respectively.
‡Energy of photons/potential energy of bubble.
§Endothermicity of reactions/potential energy of bubble.

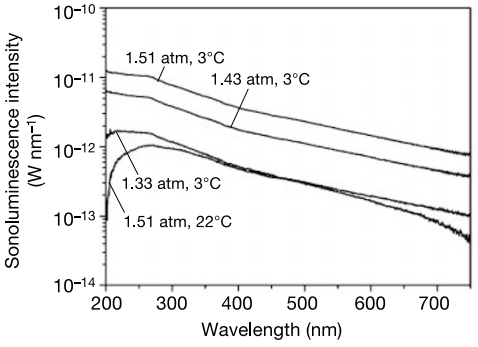

Figure 2 SBSL spectra of water collected at 52 kHz and 3 °C at acoustic intensities of 1.51, 1.43 and 1.33 atm, and at 22 °C and 1.51 atm. Quartz windows were attached to a 15-ml glass cell for better transmittance in the ultraviolet. Spectra were collected at the same acoustic intensities as chemical measurements, that is, at intensities where the bubble can be stable for a long time. Maximum SBSL intensities in the same cells can be ~2 to 3 times higher for brief periods of time. SBSL spectra were collected using a Jobin-Ivon Triax-320 monochromator with a spectrum one CCD detector (Instrument SA, 1,024 × 256 array). Spectra were corrected for light absorbance by water, quartz and the response of the optical system against NIST traceable standard lamps (OLUV-40, Optronics Lab., Inc. and EH-132 Eppley Lab). A long-pass filter was used for the data collection at wavelengths above 400 nm in order to cut off the second-order light. For absolute measurements of SBSL intensity, an OLUV-40 lamp with a neutral density filter (Oriel Corp.) was used.

Storey and Szeri conducted a detailed theoretical examination of the effect of water vapour on SBSL and sonochemistry[17], and predicted that water vapour must significantly decrease the peak temperature inside the collapsing bubble by reducing compressional heating and through endothermic chemical reactions. They calculated that the temperature inside the bubble is ~7,000 K, insufficient to cause substantial ionization of molecules, and thus did not incorporate ionization in their model[17]. Thus, SBSL can be at least partially due to broadened emission from small molecules, similar to multibubble sonoluminescence[2]. The calculated peak temperature inside the bubble does not change as the compression ratio (R_{max}/R_{min}) increases: more water is trapped inside the bubble at higher compression ratios, which counteracts the greater energy initially deposited in the larger bubble[17]. It has been found in a theoretical paper[20] that the excluded volume of the non-ideal gas results in significant suppression of the particle-producing endothermic chemical reactions within the bubble under sonoluminescence conditions. Thus, temperatures of up to 13,000 K can be achieved, which is sufficient for considerable bremsstrahlung emission.

Our data on the yield of nitrite ions during single-bubble cavitation allow us to estimate the diffusion rate of nitrogen inside the bubble and to compare it with theoretical predictions. N_2, O_2 and Ar will diffuse into a pulsating bubble in water containing dissolved air during the expansion phase. When the bubble compresses, N_2 and O_2 react under the high-temperature conditions inside the bubble and the products of these reactions dissolve in the surrounding water. This selectively leaves Ar inside the bubble, and after many pulsations the bubble will contain primarily Ar (ref. 11). Small amounts of N_2 and O_2 diffuse into the bubble during each expansion. If each molecule of nitrogen gives two molecules of nitrite ions, we can estimate a theoretical yield of nitrite ions from expected diffusion rates. Using a standard diffusion model[11], we would expect $\sim 1.2 \times 10^6$ nitrite ions per cycle to be formed in the range 3 °C to 22 °C. This is somewhat low compared to experiment (by factors of 8 and 3 at 3 °C and 22 °C, respectively), probably owing to the neglect of convective flows around the cavitating bubble, which would increase calculated rates of diffusion into the bubble.

Observation of chemical activity from single-bubble cavitation has been claimed recently by LePoint and co-workers[21,22], but these authors assert that the chemical yields were uncorrelated with the observation of sonoluminescence. Chemical activity was reported from a single bubble in an aqueous solution of carbon tetrachloride containing a mixture of sodium iodide and starch[21]; however, we observe under similar conditions that such 'bubbles' are actually droplets of CCl_4 whose presence appears to enhance the already facile oxidation of aqueous iodide. The only other report of single-bubble sonochemistry consists of the formation of solid particles (composition undetermined) during pulsation of a single bubble in an aqueous solution of carbon disulphide[22].

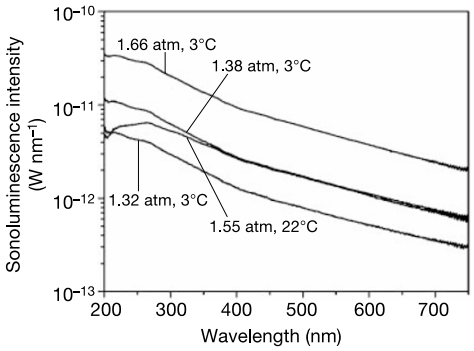

Figure 3 SBSL spectra of water collected at 28 kHz from a 100-ml quartz cell at 3 °C, 1.66 atm; 3 °C, 1.38 atm; 22 °C, 1.5 atm and 3 °C, 1.32 atm.

The paper by Taleyarkhan *et al.*[23] announcing the observation of D–D nuclear fusion during neutron-induced acoustic cavitation has proved highly controversial[24]. The authors claim the observation of neutrons and production of tritium after neutron-induced cavitation of perdeuterated acetone (C_3D_6O). Our results raise an important question. Acetone is considerably more volatile than water (30 kPa versus 3.2 kPa at 25 °C; 9.0 kPa versus 0.6 kPa at 0 °C), therefore cavitating bubbles in acetone will contain many more polyatomic molecules. The temperatures reached during cavitation will be substantially limited by the endothermic chemical reactions of the polyatomic molecules inside the collapsing bubble. We therefore expect that the extraordinary conditions necessary to initiate nuclear fusion will be exceedingly difficult to obtain in any liquid with a significant vapour pressure. However, the possibility of such events[25] in very low volatility liquids (for example, some polar organic liquids[26], molten salts or liquid metals) cannot be ruled out.

The present results show that endothermic sonochemical reactions within a collapsing bubble are a major limitation on the conditions produced during cavitation. □

Received 1 March; accepted 29 May 2002; doi:10.1038/nature00895.

1. Suslick, K. S. (ed.) *Ultrasound: Its Chemical, Physical, and Biological Effects* (VCH, New York, 1988).
2. Suslick, K. S. *Kirk-Othmer Encyclopedia of Chemical Technology*, 4th edn Vol. 26 517–541 (Wiley, New York, 1998).
3. Brenner, M. P., Hilgenfeldt, S. & Lohse, D. Single-bubble sonoluminescence. *Rev. Mod. Phys.* **74,** 425–483 (2002).
4. Putterman, S. J. & Weninger, K. R. Sonoluminescence: How bubbles turn sound into light. *Annu. Rev. Fluid Mech.* **32,** 445–476 (2000).
5. Gaitan, D. F., Crum, L. A., Church, C. C. & Roy, R. A. Sonoluminescence and bubble dynamics for a single, stable, cavitation bubble. *J. Acoust. Soc. Am.* **91,** 3166–3183 (1992).
6. Hiller, R. A., Putterman, S. J. & Weninger, K. R. Time-resolved spectra of sonoluminescence. *Phys. Rev. Lett.* **80,** 1090–1093 (1998).
7. Gompf, B. *et al.* Resolving sonoluminescence pulse width with time-correlated single photon counting. *Phys. Rev. Lett.* **79,** 1405–1408 (1997).
8. Vazquez, G., Camara, C., Putterman, S. & Weninger, K. Sonoluminescence: Nature's smallest blackbody. *Opt. Lett.* **26,** 575–577 (2001).
9. Moss, W. C., Clarke, D. B. & Young, D. A. Calculated pulse widths and spectra of a single sonoluminescing bubble. *Science* **276,** 1398–1401 (1997).
10. Hilgenfeldt, S., Grossmann, S. & Lohse, D. A simple explanation of light emission in sonoluminescence. *Nature* **398,** 402–405 (1999).
11. Lohse, D. & Hilgenfeldt, S. Inert gas accumulation in sonoluminescing bubbles. *J. Chem. Phys.* **107,** 6986–6997 (1997).
12. Makino, K., Mossoba, M. M. & Riesz, P. Chemical effects of ultrasound on aqueous solutions. Evidence for OH and H by spin trapping. *J. Am. Chem. Soc.* **104,** 3537–3539 (1982).
13. Mead, E. L., Sutherland, R. G. & Verrall, R. E. The effect of ultrasound on water in the presence of dissolved gases. *J. Phys. Chem.* **54,** 1114–1120 (1976).
14. Tian, Y., Ketterling, J. A. & Apfel, R. E. Direct observation of microbubble oscillations. *J. Acoust. Soc. Am.* **100,** 3976–3978 (1996).
15. Mark, G. *et al.* OH radical formation by ultrasound in aqueous solutions. Part 2: Terephthalate and Fricke dosimetry and the influence of various conditions on the sonolytic yield. *Ultrason. Sonochem.* **5,** 41–52 (1998).
16. Zel'dovich, Ya. B. & Raizer, Yu. P. *Physics of Shock Waves and High-Temperature Hydrodynamic Phenomena* (Academic, New York, 1966).
17. Storey, B. D. & Szeri, A. J. Water vapour, sonoluminescence and sonochemistry. *Proc. R. Soc. Lond. A* **456,** 1685–1709 (2000).
18. Barber, B. P. *et al.* Defining the unknowns of sonoluminescence. *Phys. Rep.* **281,** 65–143 (1997).
19. Margulis, M. A. Modern views on the nature of acousto-chemical reactions. *Russ. J. Phys. Chem.* **50,** 1–18 (1976).
20. Toegel, R., Hilgenfeldt, S. & Lohse, D. Suppressing dissociation in sonoluminescing bubbles: The effect of excluded volume. *Phys. Rev. Lett.* **88,** 34301-1–34301-4 (2002).
21. Lepoint, T., Lepoint-Mullie, F. & Henglein, A. in *Sonochemistry and Sonoluminescence* (eds Crum, L. A., Mason, T. J., Reisse, J. L. & Suslick, K. S.) 285–290 (Kluwer Academic, Dordrecht, 1999).
22. Verraes, T., Lepoit-Mullie, F., Lepoint, T. & Longuet-Higgins, M. S. Experimental study of the liquid flow near a single sonoluminescent bubble. *J. Acoust. Soc. Am.* **108,** 117–125 (2000).
23. Taleyarkhan, R. P. *et al.* Evidence for nuclear emissions during acoustic cavitation. *Science* **295,** 1868–1873 (2002).
24. Levi, B. G. Skepticism greets claim of bubble fusion. *Phys. Today* **55(4),** 16–18 (2002).
25. Moss, W. C., Clarke, D. B., White, J. W. & Young, D. A. Sonoluminescence and the prospects for table-top micro-thermonuclear fusion. *Phys. Lett. A* **211,** 69–74 (1996).
26. Didenko, Y. T., McNamara, W. B. III & Suslick, K. S. Molecular emission from single-bubble sonoluminescence. *Nature* **407,** 877–879 (2000).
27. McLean, J. R. & Mortimer, A. J. A cavitation and free radical dosimeter for ultrasound. *Ultrasound Med. Biol.* **14,** 59–64 (1988).

28. Field, L. & Engelhardt, P. R. Organic disulfides and related substances. XXX. Preparations and reactions of mercaptoterephthalic acids and derivatives. *J. Org. Chem.* **35,** 3647–3654 (1970).
29. Fang, X., Mark, G. & von Sonntag, C. OH radical formation by ultrasound in aqueous solutions. Part 1: the chemistry underlying the terephthalate dosimeter. *Ultrason. Sonochem.* **3,** 57–63 (1996).
30. Damiani, P. & Burini, G. Fluorometric determination of nitrite. *Talanta* **33,** 649–652 (1986).
31. Matula, T. J. *et al.* The acoustic emission from single-bubble sonoluminescence. *J. Acoust. Soc. Am.* **103,** 1377–1382 (1998).

Acknowledgements

We thank W.B. McNamara III for discussions. This work was supported by the US Defense Advanced Research Project Agency and in part by the National Science Foundation. We thank the UIUC Laboratory for Fluorescence Dynamics for use of their facilities.

Competing interests statement

The authors declare that they have no competing financial interests.

Correspondence and requests for materials should be addressed to K.S.S. (e-mail: ksuslick@uiuc.edu).

Equilibrium lithium transport between nanocrystalline phases in intercalated TiO_2 anatase

M. Wagemaker*, A. P. M. Kentgens† & F. M. Mulder*

* *Interfaculty Reactor Institute, Delft University of Technology, Mekelweg 15, 2629 JB Delft, The Netherlands*
† *NSR Center for Molecular Design, Synthesis and Structure, Department of Physical Chemistry/Solid-state NMR, University of Nijmegen, Toernooiveld 1, 6525 ED Nijmegen, The Netherlands*

Microcrystalline TiO_2 with an anatase crystal structure is used as an anode material for lithium rechargeable batteries[1,2], and also as a material for electrochromic[3–6] and solar-cell devices[7,8]. When intercalated with lithium, as required for battery applications, TiO_2 anatase undergoes spontaneous phase separation into lithium-poor ($Li_{0.01}TiO_2$) and lithium-rich ($Li_{0.6}TiO_2$) domains on a scale of several tens of nanometres[9]. During discharge, batteries need to maintain a constant electrical potential between their electrodes over a range of lithium concentrations. The two-phase equilibrium system in the electrodes provides such a plateau in potential, as only the relative phase fractions vary on charging (or discharging) of the lithium. Just as the equilibrium between a liquid and a vapour is maintained by a continuous exchange of particles between the two phases, a similar exchange is required to maintain equilibrium in the solid state. But the time and length scales over which this exchange takes place are unclear. Here we report the direct observation by solid-state nuclear magnetic resonance of the continuous lithium-ion exchange between the intermixed crystallographic phases of lithium-intercalated TiO_2. We find that, at room temperature, the continuous flux of lithium ions across the phase boundaries is as high as $1.2 \times 10^{20}\ s^{-1}\ m^{-2}$.

We used ^{7}Li magic-angle-spinning (MAS) solid-state NMR, because this microscopic probe gives information on structure and dynamics[10,11]. The anatase starting material had a particle size of ~10 μm (nitrogen BET specific surface area $<0.5\ m^2\ g^{-1}$). In Fig. 1, the central part of the ^{7}Li MAS NMR spectrum of a lithium-intercalated sample, $Li_{0.12}TiO_2$, is shown. In this sample, two phases coexist[9]: the lithium-poor phase $Li_{0.01}TiO_2$ with the anatase structure (space group $I41/amd$), and the lithium-rich phase indicated by lithium titanate ($Li_{0.6}TiO_2$; space group $Imma$). The Li in anatase gives a sharp line in addition to the broad Li in titanate signal.

The exchange of Li between the two phases is established by performing two-dimensional exchange measurements[12]. This technique effectively measures the spectrum of the ^{7}Li atoms at $t = 0$ s, then waits a 'mixing time' t_{mix}, and subsequently measures the spectrum of the same ^{7}Li atoms again at $t = t_{mix}$. The results of such measurements are shown in Fig. 2. The signal occurring on the diagonal in the plots represents ^{7}Li atoms that have the same spectrum before and after t_{mix}—that is, ^{7}Li that remained in the same crystallographic phase. The spectral intensity produced by ^{7}Li that is located in anatase at $t = 0$ and in titanate at $t = t_{mix}$ (or *vice versa*) is at the corresponding off-diagonal positions. The ridges in Fig. 2b are off-diagonal signals of this type; they are strong because of the large amount of Li that has exchanged between the two phases within the diffusion time of $t_{mix} = 50$ ms.

In Fig. 2a $t_{mix} = 50$ μs, which means virtually no diffusion time, and thus no exchange. Because about 40% of the intensity in the sharp peak in Fig. 2a is transferred to intensity in the ridges in Fig. 2b, about 40% of the initial amount of ^{7}Li in anatase has exchanged with ^{7}Li in the titanate phase after $t_{mix} = 50$ ms, as can be seen when comparing Fig. 2a and b. In Fig. 2c, a measurement is shown at 148 K using a t_{mix} of 50 ms. At this temperature the Li motion between anatase and titanate is frozen. But there still appears to be diffusion within the titanate phase; this will be due to the low activation energy for hopping between sites within this phase[9]. The measurement is shown here to prove that the cross-signal intensities in Fig. 2b cannot arise from spin diffusion due to the presence of dipolar couplings (these are suppressed by MAS).

Faster one-dimensional experiments were performed to quantify the exchange in terms of the magnetization of Li in anatase as a function of t_{mix} and temperature T. The technique is described in Fig. 3 legend. The experimental results in Fig. 3 are given as a function of t_{mix}, and for several temperatures. The data are analysed using the solution of Fick's law of diffusion, $\partial m(\mathbf{r},t)/\partial t = \nabla\cdot\{D(\mathbf{r})m(\mathbf{r},t)\}$, where $m(\mathbf{r},t)$ is the magnetization of Li at position $\mathbf{r}$ and t, and D is the Li diffusivity. Best results were obtained with

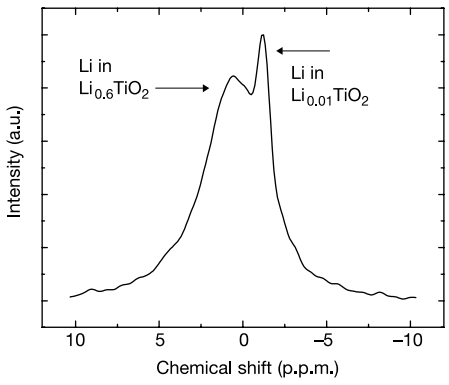

Figure 1 Central part of the ^{7}Li magic-angle-spinning NMR spectrum of $Li_{0.12}TiO_2$ at 100 °C, showing the resonances of Li in the two coexisting phases. A spinning speed of 20,000 ± 3 Hz and a radio-frequency field strength corresponding to a ^{7}Li spin nutation frequency of 192 kHz was used on a Chemagnetics 600 spectrometer. Two phases are coexisting in thermal equilibrium: a Li-poor anatase phase with a composition of $Li_{0.01}TiO_2$ (narrow peak) and a Li-rich titanate phase with composition $Li_{0.6}TiO_2$ (this peak is homogeneously broadened, with the transverse relaxation time T_2 giving its linewidth, indicating that the ^{7}Li in this phase are all experiencing similar environments).